US CLIVAR Climate Variability & Predictability

VARIATIONS

Winter 2014 • Vol. 12, No. 1

Diagnosing temperature and precipitation extremes

Mathew Barlow
University of Massachusetts Lowell, Guest Editor

Extreme events have large societal impacts and are an important part of understanding the effects of climate change. Short-term events lasting less than a week can have important impacts but are not well-represented by typical monthly or seasonal analyses. To focus on these events and their dynamics, US CLIVAR established a working group in 2012 on the large-scale meteorological patterns (LSMPs) associated with short-term extremes of temperature and precipitation for North America. The large-scale patterns can be well-resolved in current models and observational data, and allow for an assessment of model dynamics as well as the possibility of downscaling. Two key motivating questions are: what are the dynamics of these events and how well do current models capture the dynamics?

The working group held a workshop in Berkeley, CA in August 2013, with an emphasis on combining the areas of statistics, observational data, modeling, and dynamics to explore methodologies for identifying and analyzing the large-scale patterns and to identify key issues.

Extreme precipitation events: Data issues and meteorological causes

Kenneth E. Kunkel[1,2] and David R. Easterling[2]

[1]NOAA Cooperative Institute for Climate and Satellites, North Carolina State University
[2] National Climatic Data Center

Numerous papers have documented an increase in extreme precipitation events in the US over the past 30 years or so. The fundamental cause of this trend is a subject of active research. The purpose of this study is to examine the meteorological factors that underlie the trend, specifically to determine the contributions of the major types of meteorological precipitation-producing systems to the observed secular variations in heavy precipitation event frequencies. The analysis of the meteorological causes covers the period of 1908-2009.

A set of 930 long-term stations from the US National Weather Service's Cooperative Observer Network (COOP), distributed throughout the US, is used to identify extreme daily heavy precipitation events. A recent project has undertaken the keying of pre-1948 data, which hitherto has been mostly in paper form only (Dupigny-Giroux et al. 2007). A subsequent project has undertaken the quality control of the newly-keyed data (Kunkel et al. 2005). The dataset used for identification of extreme precipitation events is a combination of this newly-available quality-controlled data and the post-1947 data that has been routinely quality-controlled through the years by the National Climatic Data Center.

Extreme events are defined as daily precipitation totals exceeding the threshold for a 1 in 5 year recurrence. A total of 18,322 events are examined. The meteorological cause of each event is identified as one of the following: extratropical cyclone near a front (ETC-FRT), extratropical cyclone not near a front (ETC-NFRT), tropical cyclone (TC), mesoscale convective system (MCS), air mass convection (AMC), North American Monsoon (NAM), and upslope flow (USF). The effort has been intensive, because the assignment of a cause is done by expert judgment using several supporting pieces of information, including surface pressure fields

IN THIS ISSUE

The papers in this issue are from presentations at the workshop and represent the four focus areas. Kenneth Kunkel and David Easterling begin with an overview of data issues and meteorological causes for extreme precipitation. Richard Katz and Richard Grotjahn provide an example of conditional extreme value analysis applied to California temperature extremes. William Gutowski and John Cassano demonstrate how the Self-Organizing Maps (SOM) technique can be used to analyze LSMPs. Anthony Broccoli and Paul Loikith use a compositin0g approach to analyze the LSMPS associated with daily temperature extremes in both observations and CMIP5. Robert Black and co-authors analyze cold season temperature extremes and their links to low frequency modes of climate variability in both observations and CMIP5 model simulations. Finally, Randall Dole and coauthors conduct a case study of the March 2012 heat wave, estimating the relative contributions from trend, boundary conditions, and initial conditions. Together, these papers highlight the importance of combining the four focus areas and demonstrate the utility of the LSMP methodology.

The Working Group members are currently working on two review papers on this subject.

US CLIVAR VARIATIONS

Editor: Mike Patterson, Director
US CLIVAR Project Office
1201 New York Ave. NW Suite 400
Washington, DC 20005
202.787-168 www.usclivar.org

from reanalysis, maps of surface temperature and precipitation, the Daily Weather Map series, and tropical cyclone tracks from the North Atlantic Hurricane Database (HURDAT). Once individual station events have been assigned a cause, regional and national statistics are computed using a gridded version of the station cause assignments, so as not to overweight regions with higher densities of stations (see Kunkel et al. 2012 for details).

The percentage of events ascribed to each cause are 54% for ETC-FRT, 24% for ETC-NFRT, 13% for TC, 5% for MCS, 3% for NAM, 1% for AMC, and 0.1% for USF (Fig. 1). Altogether the two ETC types and TCs account for 90% of the extreme events. As might be expected, there are substantial regional variations in the dominant causes of extreme events (Fig. 2).

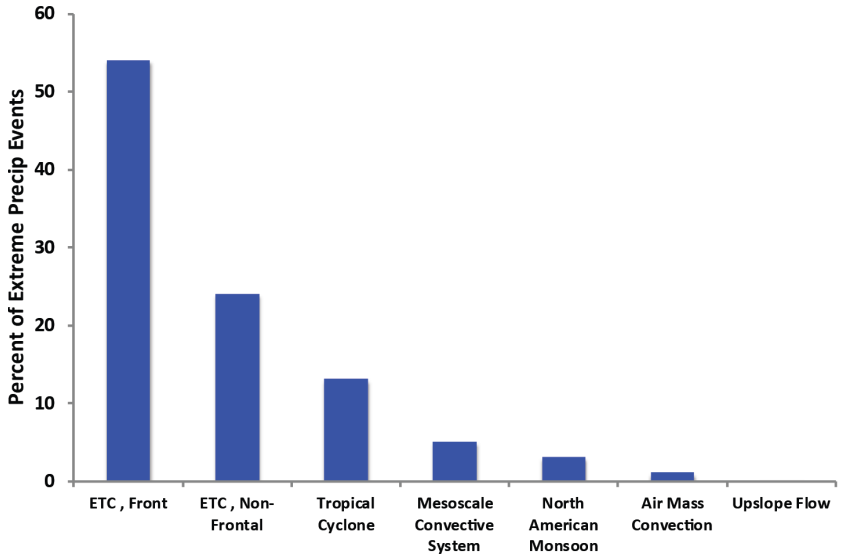

Fig. 1 The fraction (%) of extreme precipitation events assigned to each meteorological cause. "ETC" = extratropical cyclone.

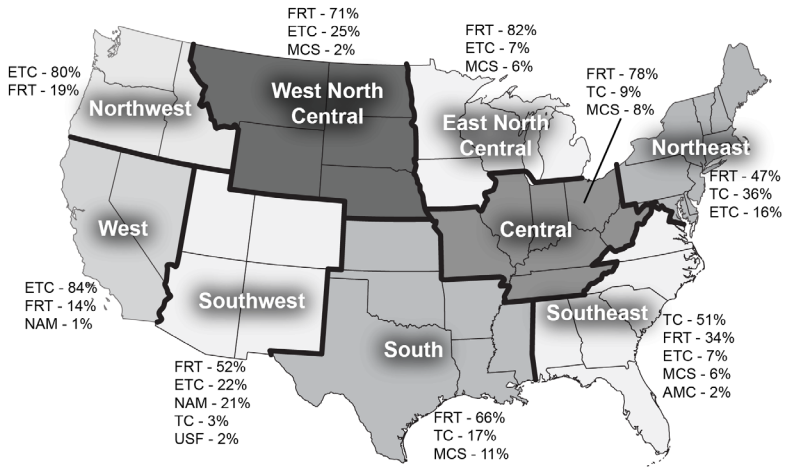

Fig. 2 Regional frequency (%) of the meteorological types associated with the occurrence of extreme precipitation events for 1908-2009 (from Kunkel et al. 2012).

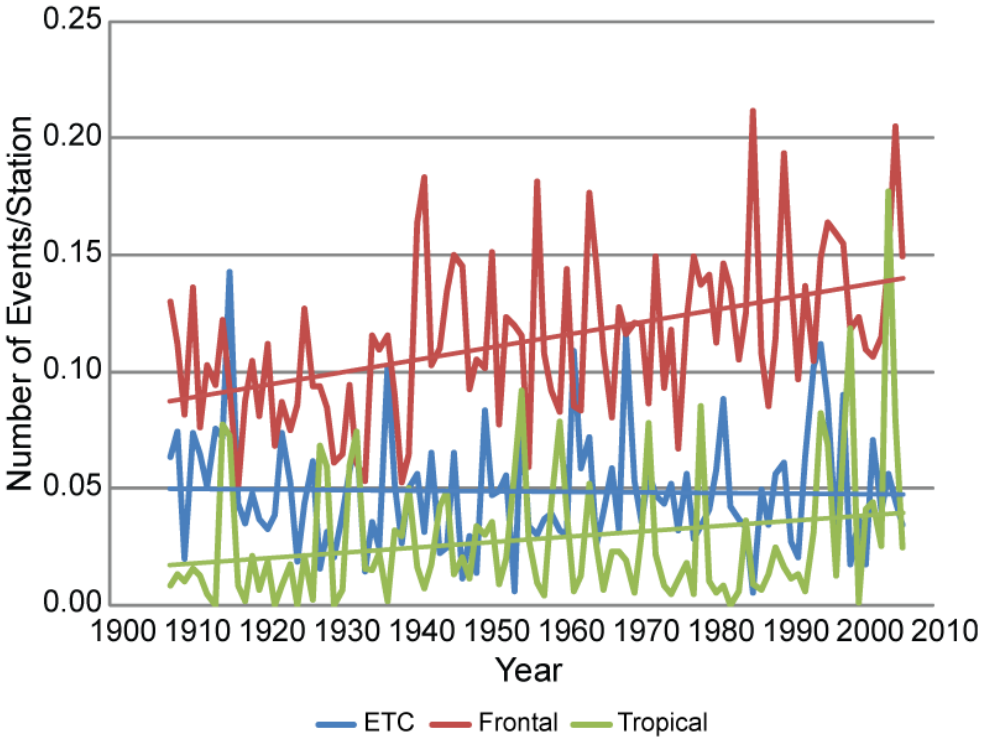

Fig. 3 Annual time series of the number of extreme events per station caused by ETCs (blue), fronts (red), and tropical cyclones (green) (from Kunkel et al. 2012).

In the Northwest and West regions, ETCs account for 80% or more of the events. The FRT category is the dominant cause in the remaining regions with the exception of the Southeast where TCs are the most frequent cause. MCSs are most common in the West North Central and East North Central where they are the 3rd most frequent cause. TCs are a prominent cause in the Northeast and South, as well as the Southeast. The NAM is responsible for 21% of the events in the Southwest. The minor categories of AMC and USF occur primarily in the Southeast (2%) and Southwest (2%), respectively.

The overall upward trend in the frequency of extreme events is primarily a warm season phenomenon, and concentrated in the late summer/early fall (Kunkel et al. 2012). In fact, the entire annual trend is explained by increases in the 5-month warm season period of June through October. The upward trend is largely driven by increases in events associated with fronts (ETC-FRT) and tropical cyclones (Fig. 3). Statistically significant upward trends in the frontal category are found in five of the nine regions: Northeast, East North Central, Central, West North Central, and South.

Given the overall upward trend in total events and in events caused by fronts and tropical cyclones, a question arises whether there are more systems causing extreme events or whether there are more extreme events per system. For fronts, there is no climatology of fronts that is suitable for detection of trends in either the number or strength of fronts. For tropical cyclones, analysis of US landfalling events does not indicate a trend (e.g., Landsea 2005). An analysis of the average number of station events that occur within the same large precipitation field associated with individual meteorological systems suggests that there has been an increasing trend in the number of extreme events per meteorological system (Kunkel et al. 2012).

The dataset of cause assignments is available from the authors. An updating of the dataset through 2013 is currently being performed.

References

Dupigny-Giroux, L.-A., T. F. Ross, J. D. Elms, R. Truesdell, and S. R. Doty, 2007: NOAA's Climate Database Modernization Program: Rescuing, archiving, and digitizing history. *Bull. Amer. Meteor. Soc.*, **88**, 1015–1017, doi: 10.1175/BAMS-88-7-1015.

Kunkel, K. E., D. R. Easterling, K. Hubbard, K. Redmond, K. Andsager, M. Kruk, and M. Spinar, 2005: Quality control of pre-1948 cooperative observer network data. *J. Atmos. Oceanic Technol.*, **22**, 1691–1705, doi: 10.1175/JTECH1816.1.

Kunkel, K. E., D. R. Easterling, D. A. R. Kristovich, B. Gleason, L. Stoecker, and R. Smith, 2012: Meteorological causes of the secular variations in observed extreme precipitation events for the conterminous United States. *J. Hydromet.*, **13**, 1131-1141, doi: 10.1175/JHM-D-11-0108.1.

Landsea, C. W., 2005: Hurricanes and global warming. *Nature*, **438**, E11–E12, doi:10.1038/nature04477.

Statistical methods for relating temperature extremes to Large-Scale Meteorological Patterns

Richard W. Katz[1] and Richard Grotjahn[2]

[1]National Center for Atmospheric Research
[2]University of California at Davis

Introduction: There is a long tradition of using statistical methods based on extreme value theory to estimate the probability of, or return levels for, extreme weather and climate events (Gumbel 1958). Because only a single static probability distribution is used, these methods can be termed unconditional extreme value analysis. In recent years, at least a few papers have made use of statistical methods based on extreme value theory to detect trends in the frequency and intensity of extreme weather and climate events; that is, allowing the extremal distribution to gradually shift over time (Brown et al. 2008).

Only rarely have extreme value distributions for weather and climate extremes been fitted conditional on indices of atmospheric or oceanic circulation, whether climate modes such as the El Niño-Southern Oscillation phenomenon or large-scale meteorological patterns (LSMPs) (Brown et al. 2008). Because the extreme value distribution randomly shifts depending on the value of the circulation index, such methods could be termed conditional extreme value analysis. Using time series of daily maximum temperature for a set of stations in the California Central Valley, we will demonstrate how indices of LSMPs can be incorporated into a conditional extreme value analysis for high temperature extremes.

Unconditional extreme value analysis: Classical extreme value analysis involves single (or static) probability distributions (i.e., that do not evolve over time). The Extremal Types Theorem, based on the concept of "max stability," states that the limiting distribution of the maximum of a sequence of random variables, suitably normalized, is the generalized extreme value (GEV) (Coles 2001). Here, as we shall see, the sequence of random variables need not be temporally independent. Further, conditional extreme value analysis (to be discussed next) provides one avenue for relaxing the assumption that the random variables be identically distributed.

The GEV distribution has three parameters: (i) a location parameter that centers the distribution; (ii) a scale parameter that governs the spread of the distribution; and (iii) a shape parameter that governs how rapidly the upper tail of the distribution decays (by convention, a negative shape parameter indicates a bounded upper tail as would be anticipated for daily maximum temperature). The block maxima approach to unconditional extreme value analysis entails fitting the GEV distribution to observed maxima (e.g., seasonal highest daily maximum temperature).

An alternative to the block maxima approach, potentially more informative and more powerful, is the peaks over threshold (POT) approach (Coles 2001). This approach entails the statistical modeling of the two most basic components of extremes: (i) the rate of occurrence of an extreme event (e.g., exceeding a high threshold); and (ii) the intensity of a given extreme event (e.g., the excess over a high threshold or by how much it is exceeded). The so-called Law of Small Numbers implies that the frequency of occurrence of sufficiently rare extreme events should have approximately a Poisson distribution, and extreme value theory implies that the excess over a sufficiently high threshold should have approximately a generalized Pareto (GP) distribution (Coles 2001). The Poisson distribution has a single rate parameter that equals both its mean and variance, and the GP distribution has two parameters: (i) a scale parameter that governs the "size" of the excesses; and (ii) a shape parameter with the same interpretation as that of the GEV distribution.

Conditional extreme value analysis: The basic idea of conditional extreme value analysis is to allow the extremal distribution to be dynamic; that is, shifting depending on the observed value of an index of a climate mode or of an LSMP. For example, Sillmann et al. (2011) analyzed the lowest winter temperature at grid points in Europe for a reanalysis product and for climate model simulations. The GEV distribution was fitted conditional on the value of an index of North Atlantic atmospheric blocking, with the location and scale parameters varying as functions of the index. In statistical terminology, the conditioning variable (e.g., a blocking index) is called a covariate.

Similarly, the distributions in the POT approach can be conditioned on an LSMP index. In our application to California

temperature extremes, the log-transformed rate parameter of the Poisson distribution and the log-transformed scale parameter of the GP distribution will both be varied as linear functions of an LSMP index (the logarithmic transformation is applied to constrain the parameters to be positive), with the shape parameter of the GP being held constant.

Application to California temperature extremes: The climate data consist of time series of daily maximum temperature at three sites, Bakersfield, Fresno, and Red Bluff, in the California Central Valley during the summer season, 16 June to 15 September, over the time period 1951-2005. As a measure of how extreme the temperature is over the entire valley, we extracted the single highest temperature each day. Despite the considerable distances among these three sites, the climatological distributions of summer daily maximum temperatures are quite similar. So the valley-wide temperature extreme is not dominated by a single site.

The LSMP index is discussed in detail in Grotjahn (2011). Briefly, the index is defined by a multi-step process that begins by choosing "target dates." The target dates satisfy a set of criteria for the extreme event type of interest; here, each date (or first of consecutive dates) is when all three stations spanning the California Central Valley have surface maximum temperature anomaly at least 1.7 standard deviations above normal. These dates happen about 1% of the time. The target dates form an ensemble for each upper air field. Ensemble averages are formed of anomalies of temperature at 850hPa and meridional wind at 700hPa. These ensemble averages are the LSMPs referred to in the present paper and shown in Grotjahn and Faure (2008). The LSMPs have highly significant ridges and troughs spanning the North Pacific and across North America, where significance is determined by bootstrap resampling: comparing the ensemble mean to randomly drawn ensembles at each grid point. Consistency between the ensemble members is assessed using "sign counts" such that only select areas of the ensemble averages (where all members of the ensemble have the same sign) are used to calculate an unnormalized projection. Those select areas sample the significant ridges and troughs of the LSMPs. Finally, the daily LSMP index is a weighted average of those projections of the target ensembles onto each corresponding daily field. The weighting is chosen to optimize when index values exceed a threshold on dates matching target dates over the 1979-1988 training period. Hence, the index estimates how strongly and how similar each day's upper air fields are to the LSMPs during prior extreme events.

Fig. 1 shows a scatterplot of the highest daily maximum temperature over the California Central Valley versus the LSMP. The horizontal line on the scatterplot indicates a threshold of 110.5 °F to be used in the extreme value analysis. Diagnostics (Coles 2001) indicate that this threshold is sufficiently high to provide an adequate fit of the GP distribution to the temperature excesses. The overall scatterplot suggests a strong relationship between the index and temperature. Nevertheless, our focus is on the points above the threshold for which the nature of the relationship is less clear.

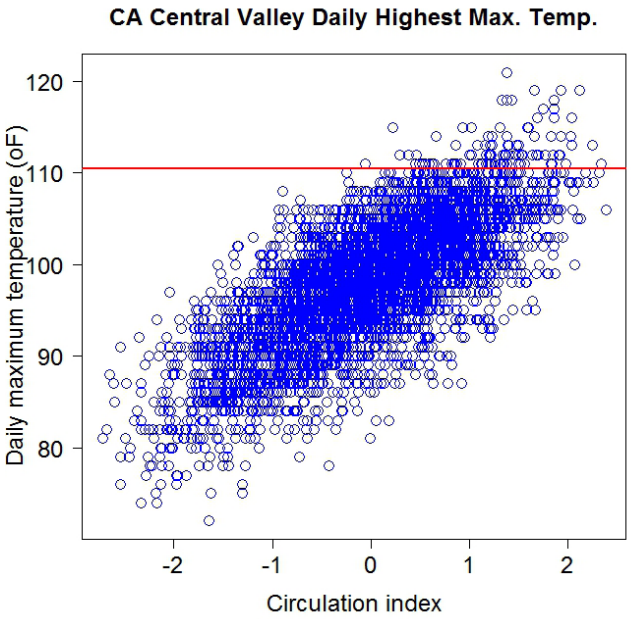

Fig. 1 Scatterplot of highest daily maximum temperature over California Central Valley (among Bakersfield, Fresno, and Red Bluff) versus an atmospheric circulation index, 16 June to 15 September, 1951-2005. Horizontal red line indicates threshold of 110.5 °F used in extreme value analysis.

To account for the marked temporal dependence of daily maximum temperature at high levels, the data have been declustered. That is, if the temperature exceeds the high threshold (in our case, 110.5 °F) on two or more consecutive days, only the single highest temperature within the cluster is used. This type of adjustment is termed "runs declustering" with declustering parameter $r = 1$ (Coles 2001). In other words, each extreme event actually corresponds to a run of consecutive days on which the maximum temperature exceeds the threshold, typically called a hot spell in the climate literature.

For simplicity, the LSMP index for the single day on which the cluster maxima occurs is used as a covariate. All of the statistical analysis was performed using functions in extRemes, an open source R package (Gilleland and Katz 2011).

Fig. 2 summarizes the results of applying the POT approach to statistically model the relationship between the highest daily maximum temperature in the California Central Valley and the LSMP index during the summer season.

The top diagram in Fig. 2 shows the fit of a Poisson distribution to the rate of clusters of daily maximum temperature exceeding the threshold, where the log-transformed rate parameter is assumed to be a linear function of the LSMP index. To aid in visualizing the goodness-of-fit, a locally smoothed version of the scatterplot is also included. The fitted statistical model clearly captures the nature of the nonlinearity in the relationship. Further, a likelihood ratio test (Coles 2001), comparing the fit of the statistical model with the LSMP index as a covariate to the fit of a single Poisson distribution, yields a P-value of virtually zero (i.e., overwhelming statistical significance).

The bottom diagram in Fig. 2 shows the fit of a GP distribution to the excess in cluster maxima over the high threshold, where the log-transformed scale parameter is assumed to be a linear function of the LSMP index. For simplicity, only the estimated median of the GP distribution is shown. It rises nonlinearly with the LSMP index, but the high degree of scatter makes it difficult to assess the nature of this relationship. Nevertheless, a likelihood ratio test (Coles 2001), comparing the fit of a GP distribution with the LSMP index as a covariate to the fit of a single GP distribution, yields a P-value of about 0.002 (i.e., strong statistical significance).

It should be noted that the LSMP index was constructed on the basis of the examination of atmospheric circulation patterns on extreme hot days in the Central Valley, using 10 out of the 55 years of data analyzed in the present paper. So these statistical tests of significance should be viewed as a confirmation of the utility of the index, not as an independent analysis.

Discussion: Our analysis has focused on high temperature clusters, where the definition of a cluster is based on statistical considerations. Hot spells or heat waves may have more complex definitions that are more meteorologically meaningful (e.g., a heat wave would not necessarily end with the maximum temperature falling below the high threshold for only one day; Meehl and Tebaldi 2004). Further, other characteristics of hot spells or heat waves, including the cluster length, should be statistically modeled as well. Initial attempts to do this include Furrer et al. (2010), which included trend components in a statistical model for hot spells or heat waves, and Photiadou et al. (2014), which included conditioning on indices of atmospheric blocking and climate modes in a similar form of statistical model.

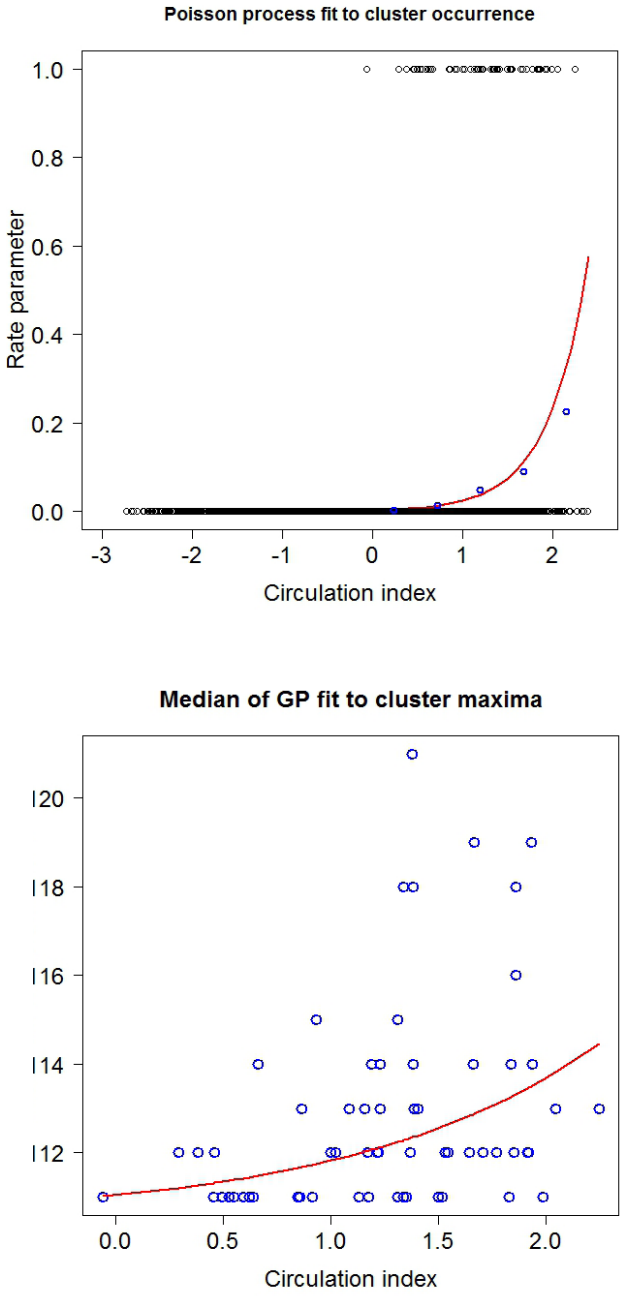

Fig. 2 Top diagram shows rate parameter of Poisson distribution (red curve) fit to occurrence of cluster of temperatures exceeding threshold of 110.5 °F (black dots: value of "1" indicates occurrence, "0" non-occurrence) with log-linear relationship to atmospheric circulation index and blue dots giving corresponding empirical rate of threshold exceedance. Bottom diagram shows median of GP distribution (red curve) fit to excess in temperature over threshold for cluster maxima (blue dots) with log-linear relationship to circulation index.

Acknowledgments

The National Center for Atmospheric Research is sponsored by the National Science Foundation. R. Grotjahn's research is supported by NSF grant 1236681.

References

Brown, S. J., J. Caesar, and C. A. T. Ferro, 2008: Global changes in extreme daily temperature since 1950. *J. Geophys. Res.*, **113**, D05115, doi: 10.1029/2006JD008091.

Coles, S., 2001: *An Introduction to Statistical Modeling of Extreme Values*. Springer, London, doi: 10.1007/978-1-4471-3675-0.

Furrer, E. M., R. W. Katz, M. D. Walter, and R. Furrer, 2010: Statistical modeling of hot spells and heat waves. *Climate Res.*, **43**, 191-205, doi: 10.3354/cr00924.

Gilleland, E., and R. W. Katz, 2011: A new software to analyze how extremes change over time. *Eos*, **92**, 13-14, doi: 10.1029/2011EO020001.

Grotjahn, R., 2011: Identifying extreme hottest days from large scale upper air data: a pilot scheme to find California Central Valley summertime maximum surface temperatures. *Climate Dyn.*, **37**, 587-604, doi: 10.1007/s00382-011-0999-z.

Grotjahn, R., and G. Faure, 2008: Composite predictor maps of extraordinary weather events in the Sacramento California region. *Wea. Forecasting*, **23**, 313-335, doi: 10.1175/2007WAF2006055.1.

Gumbel, E. J., 1958: *Statistics of Extremes*. Columbia University Press, New York.

Meehl, G., and C. Tebaldi, 2004: More intense, more frequent, and longer lasting heat waves in the 21st century. *Science*, **305**, 994-997, doi: 10.1126/science.1098704.

Photiadou, C., M. R. Jones, D. Keellings, and C. F. Dewes, 2014: Modeling European hot spells using extreme value analysis. *Climate Res.*, **58**, 193-207, doi: 10.3354/cr01191.

Sillmann, J., M. Croci-Maspoli, M. Kallache, and R. W. Katz, 2011: Extreme cold winter temperatures in Europe under the influence of North Atlantic atmospheric blocking. *J. Climate*, **24**, 5899-5913, doi: 10.1175/2011JCLI4075.1.

Self-Organizing Maps: A method for analyzing Large-Scale Meteorological Patterns associated with extreme events

William J. Gutowski, Jr.[1], and John J. Cassano[2]

[1]Iowa State University, Ames, Iowa
[2]University of Colorado, Boulder, Colorado

ntroduction: A climatological goal of extremes analysis is to extract common physical behavior across extreme events so as to gain insight into the causes and maintenance of extreme events. Depending on the phenomenon, such analysis may rely on several fields, such as mean sea-level pressure; mass, energy, moisture and momentum fluxes; and winds, temperature, humidity and geopotential heights at various atmospheric levels. One way of distilling common physical behavior from multiple fields is to form composites across many extreme events at the time of event occurrence and perhaps also at times preceding the events.

However, if there are multiple causes of extremes or if different events occur in different parts of an analysis region, then compositing all events may yield a muddled, and perhaps misleading, picture. Methods that group together events with similar characteristics can avoid this problem and potentially allow more physically relevant composites. One approach to this is Self-Organizing Maps (SOMs).

SOMs – Overview: Self-Organizing Maps (SOMs; Kohonen 1995) are two-dimensional arrays of maps that display characteristic behavior patterns of a field (e.g., Cavazos 2000; Hewitson and Crane 2002; Gutowski et al. 2004; Cassano et al. 2007). In comparison with more traditional approaches to investigating multi-dimensional data (e.g. empirical orthogonal functions) the SOM approach compares favorably (Reusch et al. 2005) with distinct advantages in interpreting underlying physical processes. SOMs can reveal observed and simulated evolution of targeted fields, including periodic behavior, provide a basis for estimating statistical significance of climate-change differences, and support conditional compositing of interacting fields and development of probability distributions. Using SOMs, one can assess physical interactions within a model and, further, determine how well a model agrees with observations for sound, physical reasons. SOMs thus give a quantitative, dynamic perspective on climatic behavior and differences between periods and data sources examined.

The SOM array is a discretization of the continuous pattern space occupied by the field examined. Fig. 1 gives an example of a SOM array of synoptic weather patterns, as defined by sea level pressure, over a region centered on Alaska. Individual maps in the array represent nodes in a projection of this continuous space onto a two-dimensional surface, with the size of the array determined by the degree of spatial discretization of the SOM space one feels is needed for the analysis at hand. The two dimensions show the two primary pattern transitions for the field examined. The input maps themselves determine the degree and types of pattern transitions, hence the "self-organizing" nature of the resulting array. The SOM node array is trained on a sequence of input maps through an artificial neural net technique. In contrast to eigenvector techniques like empirical orthogonal functions, maps in the SOM array do not necessarily favor the largest scales in the input data, but rather the scales most relevant to the field for the domain and resolution examined, with emphasis on high variance behavior. Consequently, SOMs can extract nonlinear pattern changes in fields, such as shifts in strong gradients, which may not be represented well by truncated sums of spatial modes. In addition, the pattern at each node is essentially a composite of input maps with similar spatial distribution for the field examined, so that patterns in the SOM array not only show archetypal patterns of the field examined, but they directly lend themselves to physical interpretation of actual climatic behavior.

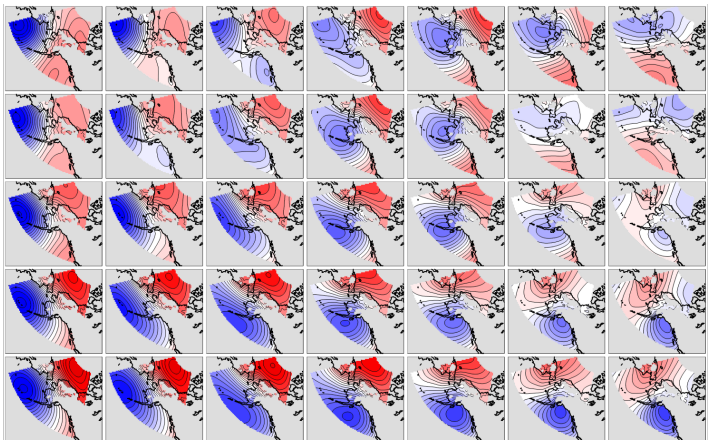

Fig. 1 Self-organizing map of synoptic weather patterns in a region focused on Alaska. The SOM array maps give the departure (in hPa) of sea level pressure (SLP) from the domain averaged SLP. The SOM used daily December-January-February (DJF) SLP for 1997-2007 from ERA-Interim reanalyses and model output. Locations with elevation exceeding 500 m are not included in the maps to avoid using SLP in regions strongly influenced by methods used to extrapolate SLP from surface pressure.

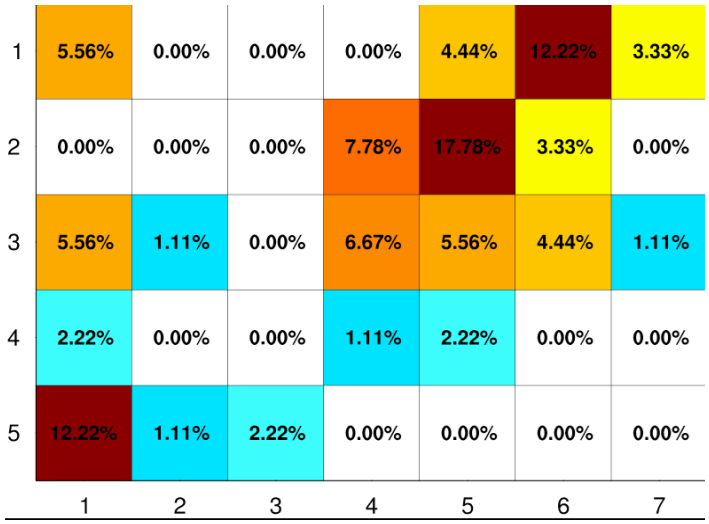

Fig. 2 Frequency in SOM space of SLP nodes accessed on days with extreme (99th percentile) precipitation during DJF. SLP for each node appears in Fig. 1.

SOM generation uses an iterative procedure that compares each member of an input sequence of maps, such as SLP (sea level pressure) or departures of SLP from its domain average, to an existing set and nudges the closest map (node) in the set toward the input map. To ensure relatively smooth transitions between SOM maps and thus retain pattern-space continuity, the procedure also nudges toward the input map all SOM nodes in a neighborhood about the best-fit node, with the degree of nudging and neighborhood size shrinking with iteration. A well-constructed SOM set is independent of initial conditions, which one can assess through tests using alternative initial conditions and sequences of map ingestion. A well-constructed SOM set minimizes the net "distance" between each input map and its nearest SOM node. For most applications, a Euclidian norm provides the "distance" separating the input map and its nearest node. The procedure producing Fig. 1 used 250,000 iterations with a set of about 2,000 input maps of daily SLP. This procedure required less than 30 minutes on a single, in-house computing node.

With a trained SOM array, one can analyze other fields as a function of each synoptic pattern identified by the SOM. For example, one can identify nodes where extreme daily precipitation events occur (Fig. 2). In this example, extreme events tend to cluster in sections of the overall SOM space, in contrast to the climatological frequency distribution, which includes all nodes and is much smoother (not shown). The clustering helps to segregate different types of extreme events.

Fig. 3 shows extreme precipitation occurring in different parts of Alaska in a manner consistent with associated SLP (Fig. 1). It is this link between large-scale synoptic weather patterns, which are reasonably well simulated by global and regional climate models, and local events that motivates this approach to study changes in extreme precipitation and temperature events in the context of large-scale features and their modulation as seen in observed and simulated behavior.

The SOM analysis extends further than simply identifying differences, however, by also allowing one to quantify the degree of agreement or disagreement between two data sets. For example, one can evaluate the degree of overlap between SOM-space frequency distributions for observed and simulated extremes. Or, by comparing simulations, one can assess the probability that a projected future climate will have more or fewer episodes with circulation patterns prone to substantial precipitation. One can construct estimates of the significance of differences through procedures such as random scrambling of each map's assigned time periods to arrive at the percent likelihood that emergent pattern differences are not simply the result of finite sampling of random patterns (Cassano et al. 2007).

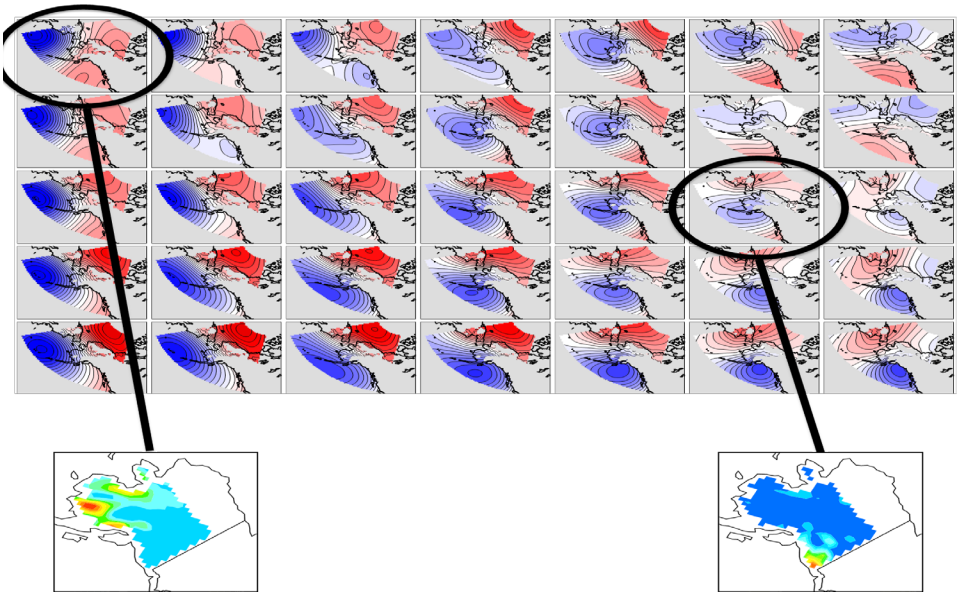

Fig. 3 Precipitation (mm/d) on two different days with extreme precipitation events (lower panels) and the SLP anomaly in SOM space (see Fig. 1) for each day, marked by the circles connected to each lower panel.

An important strength of SOM analysis is its ability to quantify time evolution. This can give additional insight on processes leading to extreme behavior. For example, we have found that days leading up to an extreme precipitation event tend to fall on nodes in the same part of SOM space as for the extreme-event day, but move rapidly to elsewhere in SOM space immediately after the event. Such slow circulation evolution allows substantial off–shore fetch to develop that supplies the moisture for an extreme event. This behavior mimics that found for central US extremes in both regional (Kawazoe and Gutowski 2013a) and global (Kawazoe and Gutowski 2013b) models. In addition, through evaluation of evolution through SOM space, one can depict the degree of agreement between observed and simulated behavior as well as features that distinguish extreme events from non-extreme events whose SLP patterns fall onto the same SOM node.

SOMs - Other examples: Application of SOMs in climate studies has occurred for several years in a variety of applications. Hewitson and Crane (2002) provide a general description of SOM analysis with details not covered here and with an illustrative application to climatological precipitation trends. Cavazos (2000) provides one of the earliest examples, using SOM analysis to explore extreme and climatological precipitation in the Balkans. Cavazos (2000) is also an example of combining several different variables (a North Atlantic Oscillation index and local values of humidity, geopotential height and thickness) to form a "map" of relationships among variables.

In contrast, more typical SOM analyses have used just one field. Gutowski et al. (2004) use monthly precipitation from observations and a simulation to evaluate the consistency of model precipitation distributions with observation. Cassano et al. (2006) use a SOM analysis of SLP to study extreme wind events at Point Barrow, Alaska. Schuenemann and Cassano (2009, 2010) also use SLP in a SOM analysis to evaluate the circulation and precipitation behavior for Greenland in a set of GCMs. Their analysis allows them to identify the GCMs that performed best

versus observed behavior and then use those GCMs to evaluate projected changes in circulation and thermodynamic factors influencing Greenland precipitation.

Typical SOM analyses use an array of many (>15) pattern maps. Feldstein (2013), however, shows that a very succinct array of only four maps can provide sufficient detail to distinguish important differences of large-scale behavior. In his case, states of the stratospheric polar vortex are identified that affect the midlatitude teleconnection response to the Madden-Julian oscillation, with attendant effects on probabilistic extreme weather forecasts.

Cautions: As with any analysis method, good practice requires thoughtful use. For example, the domain analyzed must be representative of relevant behavior. If the domain is too large, then the SOM patterns may be dominated by behavior far from the region of interest and thus reveal little about large-scale influences on extreme events. If the domain is too small, it may not adequately depict the full large-scale behavior relevant to extreme events.

The field depicted in the SOM must be relevant to the processes governing extreme events. Thus, in the extratropics, fields that depict circulation such as sea-level pressure or 500-hPa heights may be useful because they indicate important transport patterns, but 100-hPa heights may be irrelevant. Similarly, very noisy fields, such as daily precipitation, may not be useful in a SOM analysis [though longer time averages of precipitation may work well, e.g., Gutowski et al. (2004)].

As mentioned above, the SOM array represents a discretization of the field's pattern space. Too large an array may yield many SOM nodes that differ little from their neighbors and thus do little to display transitions in pattern space. One telltale sign of this would be a SOM whose frequency distribution for the full climatology has many nodes with zero frequency. Often in this case, the climatological frequency distribution of nodes accessed by the input field is rather noisy, undermining any statistical significance testing. Similarly, too small an array may not provide sufficient segregation of field behavior patterns, though the user needs to judge in terms of the targeted behavior how small an array is sufficient (cf. Feldstein 2013).

Finally, the SOM algorithm allows some degree of control on how tightly the nodes fit the patterns of the input maps. Too tight a fit can yield a SOM array of maps that do not exhibit smooth transitions through pattern space and instead may appear as a nearly random set of maps, thus undermining use of the SOM array for depicting time evolution of events.

Summary: Self-organizing maps provide a useful method for depicting typical large-scale meteorological patterns associated with extreme events. They also can help segregate different types of events and show the evolution of meteorological patterns leading into events. As with any analysis method, care is required for proper use, as noted by the cautions above.

Acknowledgments

This work benefited from discussions with Elizabeth Cassano, Steven Feldstein, Justin Glisan, Bruce Hewitson and Mark Seefeldt. Justin Glisan performed the computations yielding the figures. Support for this work came from U.S. National Science Foundation grant ARC1023369 and U.S. Department of Energy Grant DEFG0207ER64463.

References

Cassano, E.N., A.H. Lynch, J.J. Cassano, and M.R. Koslow, 2006: Classification of synoptic patterns in the western Arctic associated with extreme events at Barrow, Alaska. *Climate Res.,* **30,** 83-97.

Cassano, J.J., P. Uotila, A.H. Lynch, and E.N. Cassano, 2007: Predicted changes in synoptic forcing of net precipitation in large Arctic river basins during the 21st century. *J. Geophys. Res.,* **112,** G04S49, doi:10.1029/2006JG000332.

Cavazos, T., 2000: Using Self-Organizing Maps to investigate extreme climate events: An application to wintertime precipitation in the Balkans. *J. Climate,* **13,** 1718–1732, doi:0.1175/1520-0442(2000)013<1718:USOMTI>2.0.CO;2.

Feldstein, S., 2013: A methodology for examining the relationship between teleconnections and extreme precipitation. *Workshop on Large-Scale Meteorological Pattern Associated with Extreme Temperature and Precipitation Events*, Berkeley, CA, August 2013.

Gutowski, W. J., F. Otieno, R. W. Arritt, E. S. Takle and Z. Pan, 2004: Diagnosis and attribution of a seasonal precipitation deficit in a U.S. regional climate simulation. *J. Hydrometeor.*, **5,** 230-242, doi: 10.1175/1525-7541(2004)005<0230:DAAOAS>2.0.CO;2.

Hewitson, B. C., and R. G. Crane, 2002: Self-organizing maps: applications to synoptic climatology. *Climate Res.,* **18,** 41-57, doi: 10.3354/cr022013.

Kawazoe, S., and W. J. Gutowski, 2013a: Regional, very heavy daily precipitation in NARCCAP simulations. *J. Hydrometeor.,* **14,** 1212-1227, doi: 10.1175/JHM-D-12-068.1.

Kawazoe, S., and W. J. Gutowski, 2013b: Regional, very heavy daily precipitation in CMIP5 simulations. *J. Hydrometeor.*, **14,** 1228-1242, doi: 10.1175/JHM-D-12-0112.1.

Kohonen, T., 1995: *Self-Organizing Maps.* 2d ed. Springer-Verlag, 426 pp.

Reusch, D. B., R. B. Alley and B. C. Hewitson, 2005: Relative performance of self-organizing maps and principal component analysis in pattern extraction from synthetic climatological data. *Polar Geogr.,* **29,** 227–251, doi: 10.1080/789610199.

Schuenemann, K., and J.J. Cassano, 2009: Changes in synoptic weather patterns and Greenland precipitation in the 20th and 21st centuries. Part 1: Evaluation of late 20th century simulations from IPCC models. *J. Geophys. Res.,* **114,** D20113, doi:10.1029/2009JD011705.

Schuenemann, K. and J.J. Cassano, 2010: Changes in synoptic weather patterns and Greenland precipitation in the 20th and 21st centuries. Part 2: Attribution of the predicted change in Greenland precipitation during the 21st century. *J. Geophys. Res.,* **115,** doi:10.1029/2009JD011706.

Diagnosing Large Scale Meteorological Patterns associated with temperature extremes in models and observations

Anthony J. Broccoli[1] and Paul C. Loikith[2]

[1]Department of Environmental Sciences, Rutgers University
[2]Jet Propulsion Laboratory, California Institute of Technology

Studying the large scale meteorological patterns (LSMPs) associated with extreme temperature events presents challenges in analyzing and displaying substantial amounts of information. To produce sufficiently large samples requires the analysis of decades of observations or model output at relatively high temporal resolution, typically daily or higher. In addition, any analysis methods must be capable of capturing spatial variations in LSMPs. In this article, we briefly discuss some approaches for diagnosing LSMPs in models and observations and displaying the results. We have used these approaches in our recent studies of temperature extremes in North America (Loikith and Broccoli 2012, Loikith and Broccoli 2014).

Our analyses utilize several data sources. Daily maximum and minimum temperature anomalies are obtained from the HadGHCND data set, which is a gridded (2.5° by 3.75° latitude-longitude) product with a global domain covering the period 1950-2011 (Caesar et al. 2006). Atmospheric circulation variables are obtained from the NCEP/NCAR Reanalysis 1 (Kalnay et al. 1996), a global data set with comparable resolution (2.5° by 2.5°). Output from state-of-art climate models is obtained from historical simulations archived in association with phase 5 of the Coupled Model Intercomparison Project (Taylor et al. 2012). Our analyses use data and model output from the period 1961-1990.

The construction of composite patterns is a simple starting point for the analysis of LSMPs associated with temperature extremes. For each of the grid points of the HadGHCND data set in North America, we construct composites by averaging the spatial distribution of a chosen atmospheric variable over the days in the analysis period in which temperature anomalies are in the tails (i.e., the coldest and warmest 5%) of their frequency distribution. This analysis, which can also be performed on output from the CMIP5 models remapped to the HadGHCND grid, yields composite maps for each of the 315 grid points. Interpreting such local composites is straightforward in principle, as is comparing those extracted from models with observations, but the large number of grid points makes this approach impractical in application.

To synthesize the information from the local composites into a more succinct form, a "grand composite" is constructed from the local composites. The grand composite is constructed by first remapping each local composite to a polar coordinate grid that is referenced to the location experiencing a daily temperature extreme, then averaging these remapped local composites across all of the 315 HadGHCND grid points in North America. Examples of such grand composites are depicted in Fig. 1, which include the patterns of 500hPa geopotential height (Z500) and sea level pressure (SLP) associated with warm and cold maximum and minimum temperature extremes during January and July for observations and the multimodel ensemble mean. A metric of how well the individual local composites are represented by the grand composite is the median value of the pattern correlation between each local composite and the corresponding grand composite. The median pattern correlations range from 0.85 to 0.93 for Z500 and 0.49 to 0.78 for SLP, indicating that midtropospheric circulation patterns associated with temperature extremes are more consistent across locations than near-surface circulation patterns.

Spatial variations in the degree of similarity between the local composites and the grand composite are also of interest in determining locations in which the LSMPs associated with extreme temperatures may be distinctive. Mapping the pattern correlation between each local composite and the corresponding grand composite enables the identification of such locations. As an example, the map of pattern correlations for the SLP pattern associated with warm January maximum temperatures (not shown) indicates values above 0.5 for most of North America. In contrast, values are much lower in the southwestern United States. Examination of a local composite from this region reveals that warm January maximum temperatures are associated with high local SLP anomalies

and weak pressure gradients rather than the anomalous southerly flow implied in the grand composite. The proximity of the ocean and the barrier effect of the Rocky Mountains are important influences on extreme temperatures in this region.

The degree of symmetry between the LSMPs associated with warm and cold extremes is also of interest. As evident in a visual inspection of Fig. 1, the grand composites exhibit a high degree of symmetry, both in observations and models, with the patterns for cold extremes closely resembling those for warm extremes except for a change in sign. But do individual locations exhibit the same degree of symmetry? We address this question by developing a metric of symmetry that is simply the pattern correlation between the local composite for corresponding warm and cold extremes multiplied by -1 (so that perfect symmetry would have a value of 1). Fig. 2 depicts the symmetry metric for Z500 and SLP composites associated with January maximum temperatures in models and observations. Symmetry values are greater than 0.6 over most of North America for SLP and greater than 0.8 for Z500, with good agreement between the simulated and observed patterns. Much lower values of symmetry are noted in the southwestern United States, where a distinctive SLP pattern associated with warm January maximum temperatures was noted earlier in this article. The low values of symmetry indicate that the prevailing low-level circulation associated with warm extremes is not simply of opposite sign of the LSMP accompanying cold extremes. Such asymmetry is likely due to the influence of the nearby ocean and mountains.

Another aspect of the relationship between LSMPs and temperature extremes is whether the circulation patterns accompanying such extremes are linearly amplified versions of the patterns associated with smaller temperature anomalies. We estimate the pattern linearity for each HadGHCND grid point for January and July maximum and minimum temperatures by using circulation variables on the polar coordinate grid. First, we regress SLP and Z500 on the temperature anomalies using all days in the sample, yielding a set of regression coefficients for each variable at each point on the polar coordinate grid. The resulting regression coefficients are multiplied by the mean temperature anomaly for events in the upper and lower 5% of the temperature anomaly

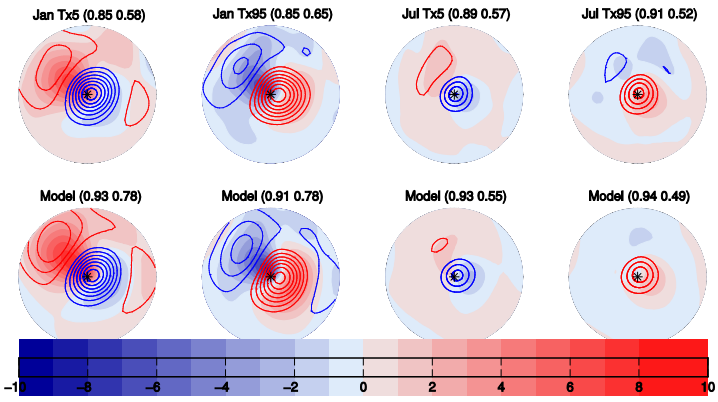

Fig. 1 Grand composites of Z500 (contours) and SLP (shading) anomalies for cold (coldest 5%) January, warm (warmest 5%) January, cold July, and warm July maximum (left to right) temperature days for observations and CMIP5 models. The top row is based on HadGHCND temperature anomalies and NCEP/NCAR Reanalysis 1 and the bottom row is the CMIP5 multi-model ensemble mean. Median pattern correlation values with individual composite patterns are given in parentheses (Z500, SLP) above each map (from Loikith and Broccoli 2014).

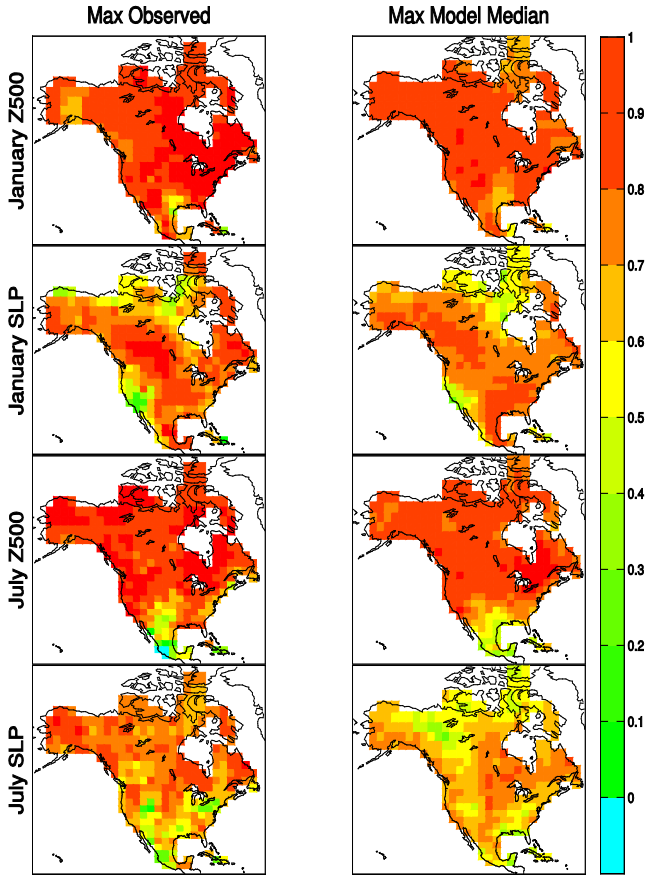

Fig. 2 Maps of symmetry of the relationship between Z500 and SLP anomalies and January and July daily maximum temperature extremes from observations and models. The model results depict the median value across all 17 models at each location (from Loikith and Broccoli 2014).

distribution to produce an estimate of what the circulation pattern for such extreme events would look like if the relationship between temperature and circulation were linear. The root-mean-square difference between the actual circulation pattern and the hypothetical linear estimate is computed and normalized by the standard deviation of the composite pattern. By this metric, a value of zero would indicate a perfect linear relationship with higher values indicative of greater nonlinearity. As defined in this way, linearity is related to symmetry (i.e., a perfectly linear pattern is perfectly symmetric) but also provides complementary information. For instance, because the linearity metric is defined separately for warm and cold extremes, it can be used to determine which tail of the distribution is contributing to asymmetry.

We use all of the analysis methods and metrics discussed in this article to develop a better understanding of the observed relationships between extreme temperature events and the LSMPs that accompany them (Loikith and Broccoli 2012). We also use these methods to evaluate the performance of state-of-art climate models in simulating such relationships (Loikith and Broccoli 2014). Future work will examine future climate simulations to determine to what extent these relationships may change in a warming climate.

References

Caesar, J., L. Alexander, and R. Vose, 2006: Large-scale changes in observed daily maximum and minimum temperatures: Creation and analysis of a new gridded data set. *J. Geophys. Res.*, **111**, D05101, doi:10.1029/2005JD006280.

Kalnay, E., and Coauthors, 1996: The NCEP/NCAR 40-Year Reanalysis Project. *Bull. Amer. Meteor. Soc.*, **77**, 437–471.

Loikith, P. C., and A. J. Broccoli, 2012: Characteristics of observed atmospheric circulation patterns associated with temperature extremes over North America. *J. Climate,* **25**, 7266–7281, doi:10.1175/JCLID-11-00709.1.

Loikith, P. C., and A. J. Broccoli, 2014: Comparison between observed and model simulated atmospheric circulation patterns associated with extreme temperature days over North America using CMIP5 historical simulations, *J. Climate*, in review.

Taylor K. E., R. J. Stouffer, and G. A. Meehl , 2012: An overview of CMIP5 and the experiment design, *Bull. Amer. Meteor. Soc.*, **93**, 485-498, doi:10.1175/BAMS-D-11-00094.1.

The low frequency modulation of anomalous temperature regimes during winter

Robert X. Black[1], Rebecca M. Westby[1] and Yun-Young Lee[2]

[1]School of Earth and Atmospheric Sciences, Georgia Institute of Technology
[2]Department of Land, Air and Water Resources, University of California, Davis

Intraseasonal anomalous temperature regime (ATR) events provide marked impacts upon the United States (Peterson et al. 2013). During winter cold air outbreaks (CAOs) and warm waves (WWs) directly affect energy consumption, local agriculture and human health leading to substantial economic effects. The regional impact of CAOs is pronounced in the South and along the mid-Atlantic coast, where Arctic air outbreaks tend to be less common (Cellitti et al. 2006). Past studies of winter ATRs have focused upon CAO events with little attention given to WW events. Although there is little evidence for the existence of long-term trends in CAO frequency, past studies do indicate that regional CAO frequency over the US is modulated by large-scale low frequency modes of variability including the Pacific-North American (PNA) teleconnection pattern, the North Atlantic (or Arctic) Oscillation (NAO) and the extratropical response to El-Nino Southern Oscillation (ENSO) (Walsh et al. 2001; Celitti et al. 2006; Lim and Schubert 2011). We review (a) an updated ATR trend analysis including a consideration of WWs, (b) a quantification of the role of low frequency modes in the regional interannual modulation of ATR frequency and (c) an assessment of CMIP5 models in representing ATR behavior including the seasonal modulation by low frequency modes (Westby et al. 2013; Lee and Black 2013). The analyses employ NCEP/NCAR reanalyses (NNR) for the period 1949 – 2011 and model output from historical CMIP5 simulations for the period 1950 – 2005.

There is no unique method for defining anomalous temperature regimes, and we choose to define events in terms of anomalies in daily-mean surface air temperature (Walsh et al. 2001). Specifically, we adopt a local metric referred to as the "impact factor" which incorporates the amplitude of the temperature anomaly. For each point (or region) considered, anomalies are defined as departures of daily-mean temperature from the (smoothed) climatological seasonal cycle during December, January and February (DJF). Prior to calculating anomalies, the daily data are first detrended by removing the long-term trend in seasonal mean temperature.

This eliminates spurious ATR trends due to regional changes in background temperature (such as the "warming hole" over the eastern US; see Westby et al. 2013 for detailed discussion of this issue). Anomalous temperature episodes are then defined as the days during each winter when the local temperature anomaly exceeds (is below) a selected threshold value, taken to be +1 (-1) standard deviation for WW (CAO) events. For each winter, the impact factor metric is defined as the following sum (over either all WW or all CAO episodes):

$$\text{Impact Factor} = \sum_{i=1}^{N} \left(\frac{T_i'}{\sigma_i} \right)$$

where T' is the local temperature anomaly, σ is the standard deviation in temperature and N is the number of days each winter above (or below) the selected threshold. The impact factor metric thereby represents a seasonally-integrated and amplitude-weighted measure of anomalous temperature episodes. This represents our seasonal metric for CAOs and WWs.

A trend analysis (not shown) reveals that there have been no statistically significant trends in either CAOs or WWs over most of the continental US during the past 60 years (Westby et al. 2013). The result for CAOs confirms earlier studies for the latter part of the 20th Century (Walsh et al. 2001) but also presents an interesting conundrum given that significant warming trends have occurred (over a similar time period) in regions of arctic air mass formation over North America (Hankes and Walsh 2011). The results are consistent with CAO behavior during recent winters (09/10; 10/11) that have been marked by prominent regional CAOs (Guirguis et al. 2011) within a background consisting of anomalously warm hemisphere-average winter temperatures (Cohen et al. 2010). This indicates that interannual ATR variability is controlled by factors besides simply changes in the mean background temperature. Interannual variations in the behavior of large-scale meteorological patterns (LSMPs) provide one such factor.

There are different physical pathways for LSMPs to influence ATR variability. In terms of dynamical processes, an LSMP pattern can directly contribute to alterations in the regional patterns of temperature advection. An LSMP can also *indirectly* contribute by providing a low frequency modulation of smaller-scale variations, such as synoptic anticyclones and cyclones, which can *directly* produce ATR events on shorter time scales. A good example of the latter influence is the modulation of midlatitude storm track behavior by large-scale atmospheric blocking patterns. There are also important local impacts of LSMPs on ATRs. For example, an LSMP can interact with local topography (e.g., cold air damming) and/or land-sea boundaries (e.g., onshore/offshore flow) to produce a small-scale response that would otherwise not exist. This kind of behavior can lead to local asymmetries between the behavior of CAOs and WWs (Loikith and Broccoli 2012). We also note that LSMP-ATR linkages are not necessarily uni-directional and it is possible for an ATR episode to feedback upon the responsible LSMP.

The local correlations between the seasonal mean impact factor and several low frequency mode measures are displayed in Fig. 1 for both CAOs (left column) and WWs (right column). It is evident that the seasonal modulation of WWs by low frequency modes is considerably more robust over the continental US than that of CAOs. Overall, the positive (negative) phase of the NAO pattern favors the occurrence of warm (cold) events in the eastern (southeastern) United States. On the other hand, the

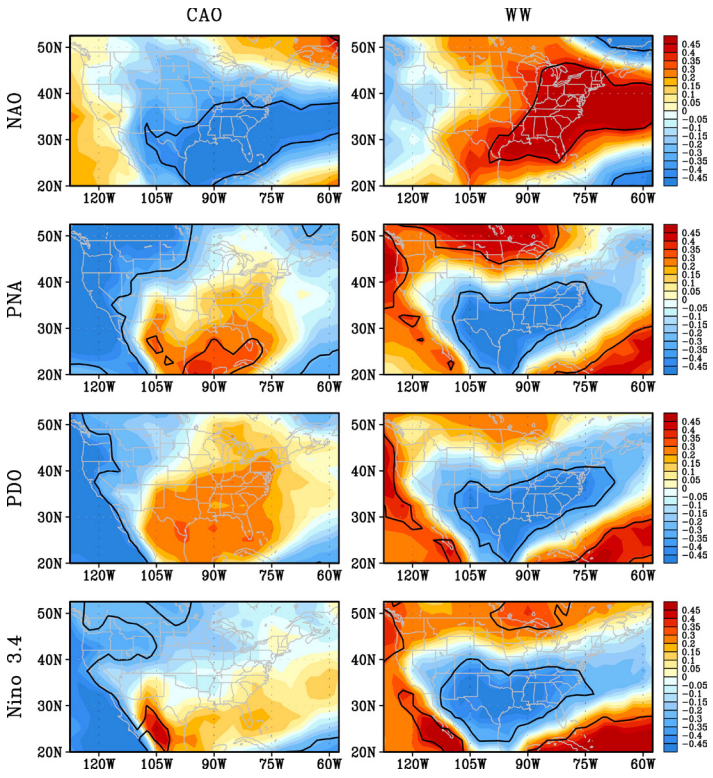

Fig. 1 Correlation between the annual impact factor of cold days (left) and warm days (right) and the NAO index (top), PNA index (upper middle), PDO index (lower middle) and Nino 3.4 index (bottom) for the period 1950–2011: closed black contours indicate statistical significance at the 95% confidence level (Figure from Westby et al. 2013; The low-frequency mode indices are from NOAA's Earth System Research Laboratory – http://www.esrl.noaa.gov/psd/data/)

negative phase of the PNA pattern tends to favor warm (cold) events over the southeastern (northwestern) US. Contrasting the results for the PNA, Pacific Decadal Oscillation (PDO) and ENSO we discover that ATR connections to climate modes are neither unique nor independent. In fact, the regional influence of the PNA pattern on ATRs resembles that of both the PDO and ENSO. Given that the midlatitude atmospheric patterns for both ENSO and the PDO have projections upon the PNA, this is not a surprising result. Over the southeast US the WW impact factor is modulated by multiple low frequency modes. A multiple linear regression analysis reveals that almost 50% of the interannual WW variability in the southeast US can be linked to the collective influence of low frequency modes (Westby et al. 2013).

In our study of CMIP5 model simulations ATR events are defined in the same manner as described above for observations. A rotated principle component analysis of monthly 500 hPa geopotential height anomalies is used to isolate the leading teleconnection patterns in CMIP5 model output (Barnston and Livezey 1987). Pattern correlation analysis is then used to select the model patterns most closely resembling the observed NAO and PNA (known as NAO-like and PNA-like patterns). PDO-like modes are identified from model output as the first loading vector of monthly mean sea surface temperature anomalies over the midlatitude North Pacific (Mantua and Hare 2002). ENSO-like modes are assessed in the model simulations in the same manner as the observed Nino-3.4 index. Last, a *k*-means clustering analysis is used to group respective model patterns into categories with similar horizontal structures (additional details of the above methods are available in Westby et al. 2013 and Lee and Black 2013).

The CMIP model analysis indicates that WW (CAO) frequency is typically overestimated (underestimated) in the models. Similar to observations, little evidence is found in the model simulations of significant regional ATR trends. The relationship between the regional ATR impact factor and low frequency modes in CMIP5 models is summarized in Fig. 2. Generally speaking, the CMIP5 models properly represent many of the observed significant associations between ATRs and low frequency modes, particularly modulation by NAO-like and PNA-like patterns. One common

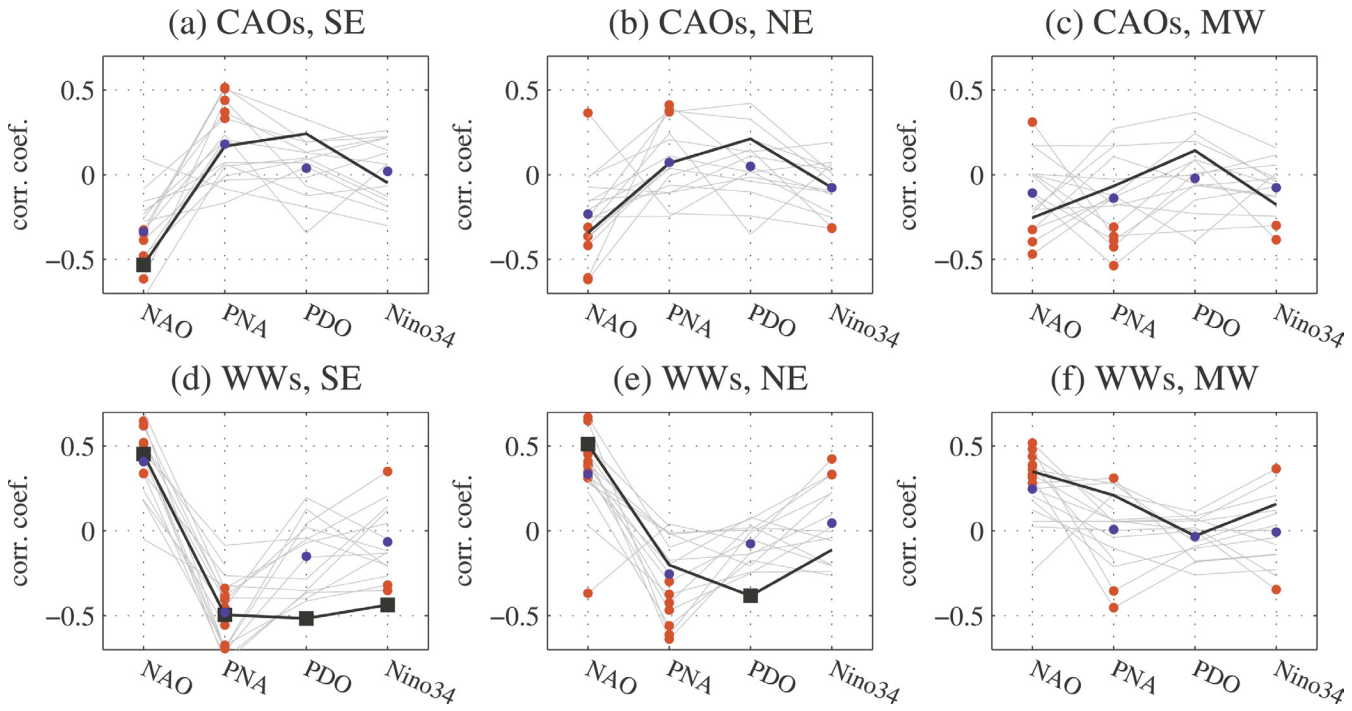

Fig. 2 Correlation between the low frequency mode indices and the annual impact factor for CAOs (top row) and WWs (bottom row) occurring in the southeast US (left column), northeast US (middle column) and upper Midwest (right column) during the period 1951–2005. Results are displayed for each of 16 CMIP5 models (gray lines) and observations (black lines). The filled red circles and black squares indicate correlation values that are statistically significant values at the 95% confidence level while the filled blue circles are the average correlation over the 16 models (figure from Westby et al. 2013).

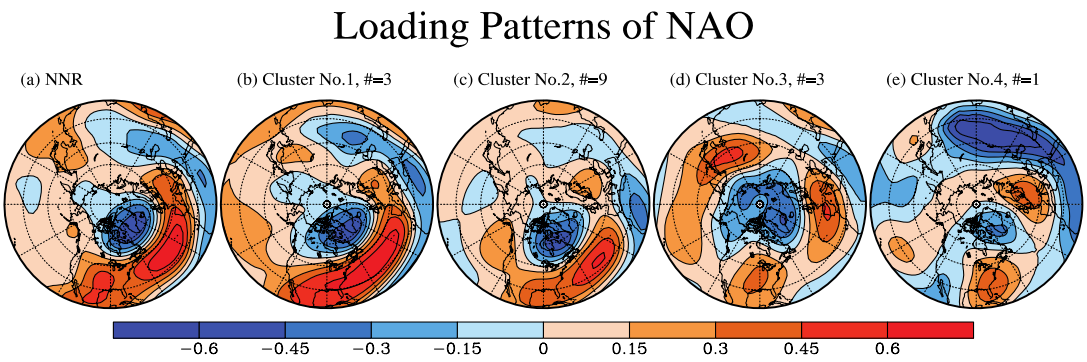

Fig. 3 Cluster-mean composites of NAO-like anomaly patterns for CMIP5 models along with observed NAO anomaly pattern (left frame). Clusters 1, 2, 3 and 4 consist of 3, 9, 3 and 1 model members respectively. The plotted field is dimensionless (figure from Lee and Black 2013).

model failure is the virtual absence of a seasonal modulation of ATRs by the PDO. This is largely due to the inadequacy of the CMIP5 models in representing the PDO (e.g., Kim et al. 2012), which is dependent on an accurate representation of atmosphere-ocean coupling processes in midlatitudes.

The CMIP5 models overall do a much better job in representing the behavior of the NAO and PNA patterns (Lee and Black 2013). Nonetheless, a small subset of CMIP5 models fails to correctly represent the structure of the NAO. This is illustrated in Fig. 3 in which cluster mean model anomaly structures are plotted alongside the observed NAO pattern (left frame). Although both clusters #1 and #2 (comprising 12 of the 16 models considered) capture the typical north-south dipole structure of the NAO over the Atlantic (albeit with differences in pole location and local amplitude), cluster #3 (3 models) has more of a hemispheric annular structure with a relatively weak and northeastward shifted Atlantic dipole feature. Cluster #4 does not resemble the observed NAO pattern at all. Lee and Black (2013) also demonstrate that such model biases in low frequency mode structure carry over to the regional misrepresentation of associated anomalous weather conditions. Thus, we conclude by suggesting that predictions in the likely future behavior of ATRs and ATR-low frequency mode linkages will ultimately be limited by the ability of coupled global climate models to properly represent the (evolving) behavior of prominent low frequency climate modes.

References

Barnston, A. G., and R. E. Livezey, 1987: Classification, seasonality and persistence of low-frequency atmospheric circulation patterns. *Mon. Wea. Rev.*, **115**, 1083–1126.

Cellitti, M. P., J. E. Walsh, R. M. Rauber, and D. H. Portis, 2006: Extreme cold air outbreaks over the United States, the polar vortex, and the large-scale circulation. *J. Geophys. Res.*, **111**, D02114, doi: 10.1029/2005JD006273.

Cohen, J. L., J. Foster, M. Barlow, K. Saito, and J. Jones, 2010: Winter 2009–2010: A case study of an extreme Arctic Oscillation event. *Geophys. Res. Lett.*, **37**, L17707, doi: 10.1029/2010GL044256.

Guirguis, K., A. Gershunov, R. Schwartz, and S. Bennett, 2011: Recent warm and cold daily winter temperature extremes in the Northern Hemisphere, *Geophys. Res. Lett.,* **38**, L17701, doi: 10.1029/2011GL048762.

Hankes, I. E., and J. E. Walsh, 2011: Characteristics of extreme cold air masses over the North American sub-Arctic. *J. Geophys. Res.*, **116**, D11102, doi: 10.1029/2009JD013582.

Kim, H.-M., P. J. Webster, and J. A. Curry, 2012: Evaluation of short-term climate change prediction in multi-model CMIP5 decadal hindcasts, *Geophys. Res. Lett.,* **39**, L10701, doi: 10.1029/2012GL051644.

Lee, Y.-Y., and R. X. Black, 2013: Boreal winter low-frequency variability in CMIP5 models. *J. Geophys. Res. Atmos.,* **118**, 6891–6904, doi: 10.1002/jgrd.50493.

Lim Y.-K., and S. Schubert, 2011: The impact of ENSO and the Arctic Oscillation on winter temperature extremes in the southeast United States. *Geophys. Res. Lett.* **38**, L15706, doi: 10.1029/2011GL048283.

Loikith, P. C., and A. J. Broccoli, 2012: Characteristics of observed atmospheric circulation patterns associated with temperature extremes over North America. *J. Climate*, **25**, 7266–7281, doi: 10.1175/JCLI-D011-00709.1.

Mantua, N. J., and S. R. Hare, 2002: The Pacific Decadal Oscillation. *J. Oceanogr.*, **58**, 35–44, doi: 10.1023/A:1015820616384.

Peterson, T. C., and Co-authors, 2013: Monitoring and understanding changes in heat waves, cold waves, floods, and droughts in the United States: state of knowledge. *Bull. Amer. Meteor. Soc.*, **94**, 821–834, doi: 10.1175/BAMS-D-12-00066.1.

Walsh, J. E., A. S. Phillips, D. H. Portis, and W. L. Chapman, 2001: Extreme cold outbreaks in the United States and Europe, 1948–99. *J. Climate*, **14**, 2642–2658, doi: 10.1175/1520-0442(2001)014<2642:ECOITU>2.0.CO;2.

Westby, R. M., Y.-Y. Lee, R. X. Black, 2013: Anomalous temperature regimes during the cool season: long-term trends, low-frequency mode modulation, and representation in CMIP5 simulations. *J. Climate*, **26**, 9061–9076, doi: 10.1175/JCLI-D-13-00003.1.

The making of an extreme event: Putting the pieces together

Randall Dole[1], Martin Hoerling[1], Arun Kumar[2], Jon Eischeid[1,3], Judith Perlwitz[1,3], Xiao-Wei Quan[1,3], George Kiladis[1], Robert Webb[1], Donald Murray[1,3], Mingyue Chen[2], Klaus Wolter[1,3], and Tao Zhang[1,3]

[1]NOAA Earth System Research Laboratory
[2]NOAA Climate Prediction Center
[3]University of Colorado, Cooperative Institute for Research in Environmental Sciences

Introduction: CLIVAR's mission is to foster understanding and prediction of climate variability and change on intraseasonal to centennial time scales. Within this broader mission, advancing understanding and predictions of climate extremes poses a specific research challenge for CLIVAR that is of fundamental societal importance (US CLIVAR 2013). Here we identify how phenomena and processes across the temporal spectrum from climate to weather contributed to a specific extreme event, the March 2012 extreme warm temperatures over the central and eastern US. We also consider the extent to which this event might have been anticipated from prior climate information. The following is a brief summary of findings, with full results presented in a paper now in press (Dole et al. 2014).

Background and climate overview: March 2012 was the warmest March on record for the contiguous US, with temperatures averaging 4.8° C above normal according to the National Climatic Data Center (NCDC). Monthly-mean anomalies reached more than +9° C in the core of the heat wave region in the upper Midwest, with daily-mean temperature anomalies during the event exceeding +22° C (40° F) at several locations. The record warm temperatures led to premature blooming of trees, flowers and crops over the eastern two-thirds of the country (Elwood et al. 2013). Major fruit crop losses occurred subsequently in parts of the upper Midwest when more seasonal freezing temperatures returned in April (Allen 2012).

When viewed in the broader global context, the extreme warm temperatures in March 2012 had a distinct regional character (Fig. 1a). Global-mean temperatures for the month were approximately 0.7° C above the 20th century average (NCDC). The North American surface temperature pattern in March 2012 had a historical precedent in an event that occurred over a century earlier (Fig. 1b). The March 1910 US temperature anomaly was +4.5° C above the twentieth century average, or 0.3° C below that of March 2012. Compared to March 1910, the global-mean temperature in March 2012 was approximately 0.9° C higher, consistent with the general increase in global-mean temperatures during the 20th century that has been attributed mostly to human influences (Hegerl et al. 2007).

Not all regions warmed at the same rate during this period (Fig. 1c), with the core of the heat wave region experiencing a long-term warming of approximately 0.5-1° C. This is within the range of warming estimated from CMIP simulations forced by increasing greenhouse gas concentrations. A first-order estimate of the effect of the warming on the event can be obtained by subtracting the temperature changes estimated from the long-term regional trend from the March 2012 temperature anomalies (Fig. 1d). The resulting detrended March 2012 temperature anomaly pattern is nearly identical to that of March 1910 over the US, with considerable similarity evident in many other regions over the globe. The close correspondence in the core of the heat wave region reflects the fact the long-term warming is approximately an order-of-magnitude smaller than the magnitude of the event anomaly. Overall, this result indicates that a superposition of a strong natural variation similar to that observed in March 1910 onto long-term warming of approximately 0.5-1° C would be sufficient to account for the extreme magnitude of the March 2012 US temperature anomalies.

Contributions from seasonal-to interannual and subseasonal variability: The primary proximate cause for the extreme warm temperatures was intense and sustained poleward heat associated with a Rossby wavetrain extending northward and eastward from the western tropical Pacific, with major anticyclonic centers located just east of the dateline and over the Great Lakes, the latter directly related to the extreme warm temperatures (Dole et al. 2014). The key question then becomes: what factors were primarily responsible for this anomalous circulation pattern? From a seasonal perspective, the preceding winter (December-

February) was characterized by La Niña conditions, with generally suppressed convection over the central Pacific and enhanced convection from the eastern Indian Ocean to over the Maritime Continent. This general pattern of convection intensified substantially from late February through mid-March, particularly over the western Maritime Continent in association with the slow eastward propagation of a Madden-Julian Oscillation (MJO). This constructive superposition of seasonal and intraseasonal convection patterns was followed by rapid development of the wavetrain and circulation anomalies that were directly related to the extreme warm temperatures over the US in March 2012.

Coupled model predictions for March 2012 from the NOAA/NCEP Climate Forecast System version 2 (CFSv2) initialized from late Fall 2011 through January 2012 showed very similar ensemble-mean temperature patterns, with above normal temperatures predicted over the eastern US and below normal temperatures predicted over the northwestern US, western Canada and Alaska (Dole et al. 2014). This general pattern was broadly similar to that observed in March 2012 (Fig. 1a), but with the maximum warm temperature anomalies in the model displaced eastward of the observed maximum. The high degree of consistency between ensemble predictions initialized over this period primarily reflects a forced model response to sea surface temperatures (SSTs) that were evolving on seasonal-to-interannual time scales, with the response increasing the probability of an extreme warm event over the eastern US above that estimated from the long-term warming trend.

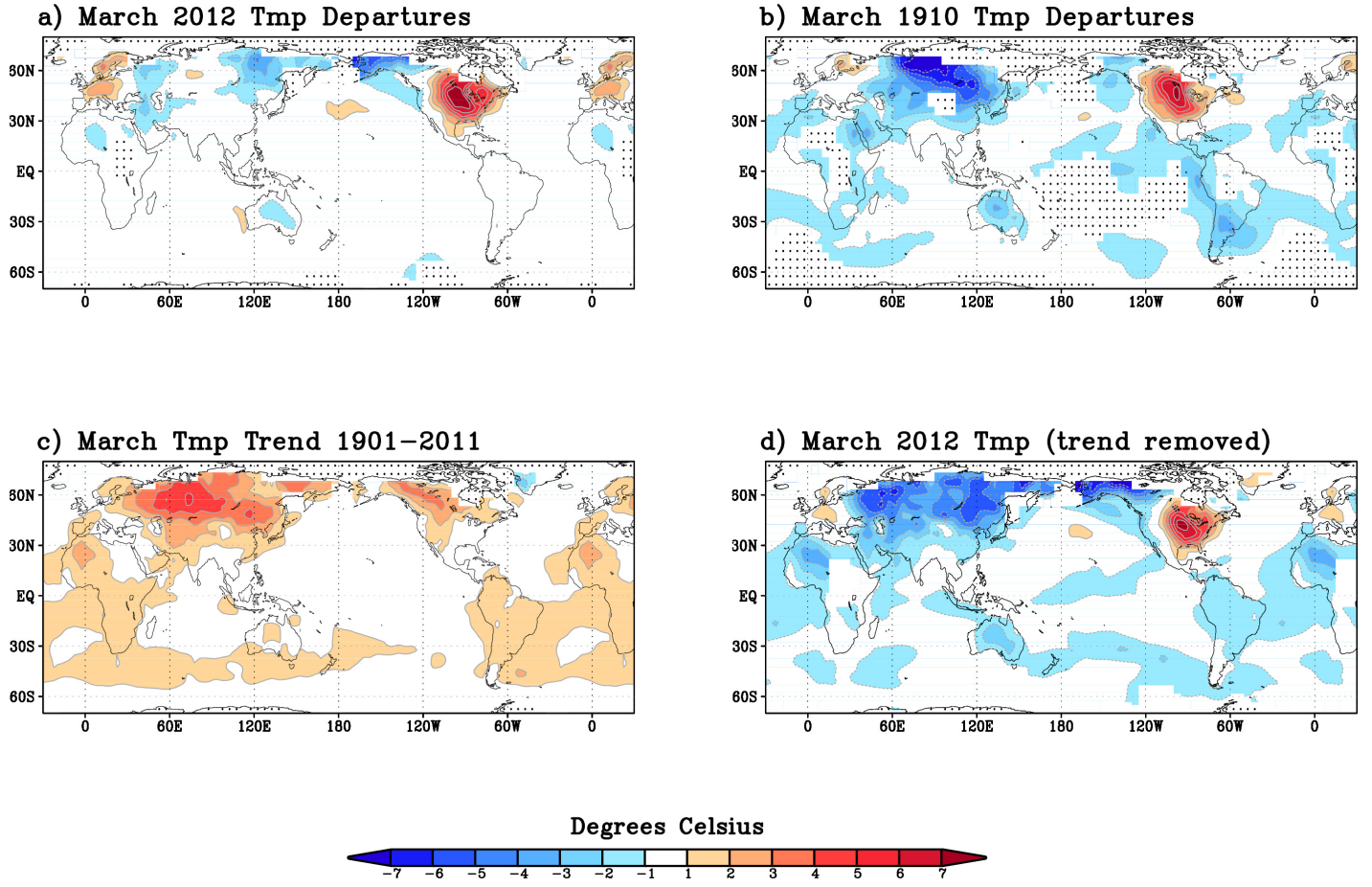

Fig. 1 March surface temperature anomalies for a) 2012 and b) 1910. c) March temperature change derived from the trend over the 111-year period 1901-2011. d) Detrended March 2012 temperature anomalies. (Units: °C). Areas of insufficient data are indicated by stippling. Data are from the NCDC merged land-ocean dataset Version 3b (Smith et al. 2008). Anomalies are departures from means over a 1981-2010 base period.

Predictions initialized in February, while sharing many common features, also had important differences from earlier runs. In particular, temperature predictions over the central and eastern US showed exceptionally strong positive anomalies (ensemble-mean temperature anomalies of approximately 2 standardized departures above the variability in model forecasts), with the epicenter of warm anomalies shifted northwestward over the Midwest closer to the pattern observed in March. The much stronger signal in the February predictions compared to predictions initialized earlier indicates that specific conditions emergent in early February, most likely in the atmospheric state, greatly increased the probability of extreme warm temperatures in March over the US and led to a predicted pattern of temperatures much closer to observed. The NOAA Climate Prediction Center capitalized on this 'forecast of opportunity' to anticipate the monthly temperature pattern very well, achieving its highest skill score to date for their March 2012 forecast for the contiguous US issued in mid-February.

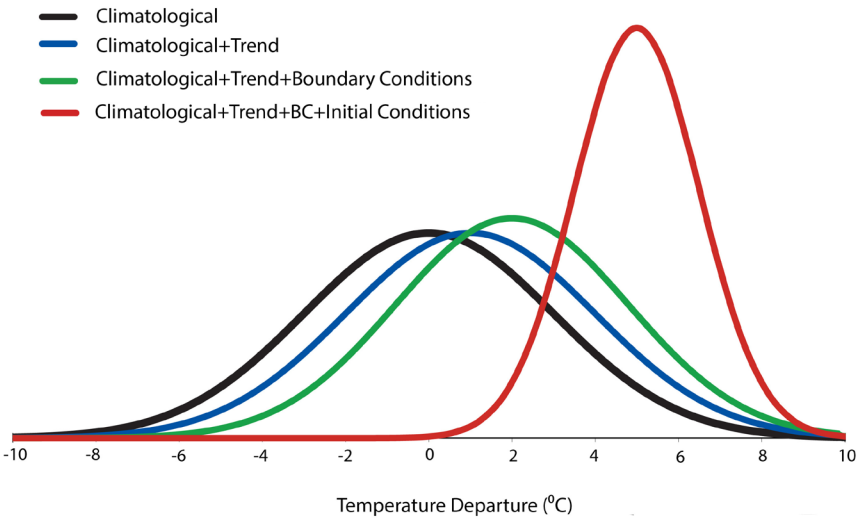

Fig. 2 A schematic representation of how predictions for the March 2012 Probability Distribution Function (PDF) shifted away from the climatological distribution (black) in response to different factors. These include long-term trends and multi-decadal variations that evolve on time scales much longer than a season (blue), SSTs and other boundary forcings varying on seasonal-to-interannual time scales (green), and the MJO and other shorter time-scale phenomena dominated by atmospheric processes varying on subseasonal-to-daily time scales (red).

Putting the pieces together: Fig. 2 illustrates schematically how multiple pieces from longer-term climate trends to shorter-term weather and climate variations contributed to extreme warm temperatures over the US in March 2012. A long-term March warming trend shifted the temperature probability distribution to the right (blue curve) from the climatological distribution (black curve) by approximately 1° C, increasing the probability of above normal temperatures and warm extremes. The addition of specific boundary conditions for 2011-2012, most likely related to tropical ocean conditions in the Indo-Pacific sector, increased the probability further (green curve). The large shift in the distribution that occurred in February associated with a strong MJO event (red curve) greatly increased the probability for an extremely warm March, and provided important additional predictive information on the timing and spatial pattern of temperature anomalies.

Thus, several pieces from climate to weather ultimately linked together favorably to produce this extreme event. The probability that March 2012 would be exceptionally warm over the US evolved dynamically as different phenomena became predictable, thereby changing the conditional probability for extreme event occurrence. However, even at lead times of a few weeks extreme warm temperatures were far from certain. As the width of the distributions indicates, a large range of outcomes was possible, and what occurred could well have been otherwise. Estimating the time-evolving effects of multiple conditions on extreme event probability presents a difficult but important research challenge, with more general implications for what information might be provided and when it might be provided for better anticipating the possibility for extreme events.

Overall, our results show that the extreme magnitude of the March 2012 warmth can be largely explained by natural variability, with an additional contribution from a long-term warming trend that is likely due mostly to human influences. Phenomena evolving on centennial, interannual, intraseasonal and synoptic weather time scales were all factors in making this event extreme. Increased understanding of the connections between climate and weather, and especially the implications for anticipating future extreme events, will be essential for meeting many societal needs. While advances have been impressive, there remain many opportunities for further progress (Shapiro et al 2010; US CLIVAR 2013). CLIVAR research can play a central role in helping to achieve major scientific advances in this area over the next decade.

References

Allen, B., 2012: Hard freeze hurts cherry crop. Environment Report. Available at http://www.environmentreport.org/show.php?showID=629

Dole, R., M. Hoerling, A. Kumar, J. Eischeid, J. Perlwitz, X-W. Quan, G. Kiladis, R. Webb, D. Murray, M. Chen, K. Wolter, and T. Zhang, 2014: The making of an extreme event: putting the pieces together. *Bull. Amer. Meteor. Soc.,* in press, doi:10.1175/BAMS-D-12-00069.1.

Elwood, E. R., S. A. Temple, R. B. Primack, N. L. Bradley, and C. C. Davis, 2013: Record-breaking early flowering in the eastern United States. *PlosOne 8*, doi: 10.1371/journal.pone.0053788.

Hegerl, G. C., F. W. Zwiers, P. Braconnot, N. P. Gillett, Y. Luo, J. A. Marengo Orsini, N. Nicholls, J. E. Penner, and P.A. Stott, 2007: Understanding and Attributing Climate Change. In: Climate Change 2007: The Physical Science Basis. Contribution of Working Group I to the Fourth Assessment Report of the Intergovernmental Panel on Climate Change [Solomon, S., D. Qin, M. Manning, Z. Chen, M. Marquis, K.B. Averyt, M. Tignor and H.L. Miller (eds.)]. Cambridge University Press, Cambridge, United Kingdom and New York, NY, USA.

Shapiro, M., and Co-authors, 2010: An Earth-System prediction initiative for the twenty-first century. *Bull. Amer. Meteor. Soc.*, **91**, 1377–1388, doi: 10.1175/2010BAMS2944.1.

Smith, T.M., R. W. Reynolds, T. C. Peterson, and J. Lawrimore, 2008: Improvements to NOAA's historical merged land-ocean surface temperature analysis (1880-2006). *J. Climate*, **21**, 2283-2296, doi:10.1175/2007JCLI2100.1.

US CLIVAR Scientific Steering Committee, 2013: *US Climate Variability and Predictability Program Science Plan.* Report 2013-7, US CLIVAR Project Office, Washington, DC 20005.

New US CLIVAR Science Plan

We are pleased to announce the publication of the new US CLIVAR Science Plan outlining the research goals and strategies for the next 15 years of the program.

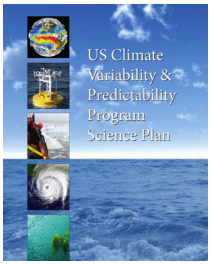

Click the figure to download or request a printed copy of the Plan.

Specifically, the Plan is intended to:

- Update the goals and priorities of US CLIVAR based on achievements to date;
- Articulate the expansion of core research to target specific research challenges;
- Emphasize strengthened ties to the broader Earth Sciences community and relevance to societal impacts;
- Bolster research funding commitments by US agencies to achieve their mission objectives; and
- Articulate the envisioned collaborations with other US and international research programs.

The Plan was developed by the US CLIVAR Scientific Steering Committee over a 2-year period with input from its panels and members of the research community. We wish to acknowledge the significant effort of over 60 contributors to help scope, draft, review, and edit the Plan. The final document reflects revisions based on an open public review held this past summer.

Two Town Halls are being held jointly with International CLIVAR to engage the community on the key components of the future US and International programs. The presentations for the first, held at the 2013 AGU Fall Meeting, are available to download here. The second, planned for the Ocean Sciences meeting, will be held on Tuesday, February 25, from 6:30-8:30pm in Room 312 at the Hawaii Convention Center. Please join us in Hawaii and learn of the future research directions and opportunities to get involved.

Call for New Panelists – Opportunity to Shape the Program's Future

The SSC seeks qualified individuals to serve on its three subsidiary panels beginning in 2014. These Panels formulate science goals and implementation strategies, catalyze and coordinate activities, and work with agencies and international partners to advance the progress of the climate research community. It is a particularly exciting time to join the Panels, as they embark on planning activities to address the goals and research challenges articulated in the recently published **US CLIVAR Science Plan**.

Consider nominating yourself or a colleague to serve. See the **Call for New Panelists** on our website for information on the expertise sought and the link to the online nomination form. Deadline for nominating is March 21.

TRANSITIONS

Thank You to Outgoing SSC and Panel Members

The US CLIVAR Scientific Steering Committee (SSC) expresses sincere gratitude to the following individuals for their years of service to planning and advancing US CLIVAR science.

SSC Members
Michael Bosilovich, Baylor Fox-Kemper, Lisa Goddard, and Jay McCreary

Phenomena, Observations, and Synthesis (POS) Panel
Nicholas Bond, Don Chambers, Simon de Szoeke, Benjamin Giese, Alexander Gershunov, Rick Lumpkin, and Rong Zhang

Process Study Model Improvement (PSMI) Panel
Michael Gregg, Meibing Jin, Sukyoung Lee, and Robert Wood

Predictability, Prediction, and Applications Interface (PPAI) Panel
Annalisa Bracco, Curtis Deutsch, Joshua Xiouhua Fu, Ron Lindsay, Cristiana Stan, and Liqiang Sun

Welcome to New 2014 SSC Members

Two Panel members accepted the SSC invitation to serve as Panel co-chairs and on the SSC starting in 2014. Welcome aboard!

Yan Xue, POS Panel Co-chair
Gad Levy, PSMI Panel Co-chair
Gregg Garfin, PPAI Panel Co-chair

Search for Project Office Program Specialist

The University Corporation for Atmospheric Research is seeking applications for the position of Program Specialist II in the US CLIVAR Project Office located in Washington DC. The incumbent will work closely with the Project Office Director to assist the US CLIVAR science community in planning and implementing coordinated research programs to achieve program goals; develop and deliver useful communication and outreach materials providing timely information on US CLIVAR science advances, programmatic directions, and new opportunities to a diverse set of audiences; and provide organizational support to facilitate interagency dialogue and enable work of US CLIVAR science planning and implementation bodies.

A Bachelor's degree in oceanography, meteorology, or earth system science plus two years of work experience related to the job duties of the position, or an equivalent combination of education and experience (such as a Master's degree and one year of experience) are required. Experience in physical climate research and background in climate science directly relevant to the US CLIVAR Program are desired.

The full announcement is available at the UCAR Current Job Openings Portal, listed under Administration as a Program Specialist II. Application deadline is Friday, March 14, 2014.

www.usclivar.org
uscpo@usclivar.org
twitter.com/usclivar

US Climate Variability and Predictability (CLIVAR) Program
1201 New York Ave. NW, Suite 400
Washington, DC 20005
(202) 787-1681

US CLIVAR acknowledges support from these US agencies:

This material was developed with federal support of NASA (AGS-0963735), NOAA (NA11OAR4310213), NSF (AGS-0961146), and DOE (AGS-1357212). Any opinions, findings, conclusions or recommendations expressed in this material are those of the authors and do not necessarily reflect the views of the sponsoring agencies.